Photoacoustic and Ac Impedance Measurements for ZnO Varistors with ZnO Nanoparticles Addition

A. Sedky [1,3], M. I. Youssif [2,5,*] and T. A. El-Brolossy [3,4]

[1]Physics Department, Faculty of science, Assiut University, Assiut, Egypt
[2]Physics Department, Faculty of Science, Damietta University, New Damietta 34517, Egypt
[3]Physics Department, Faculty of science, King Faisal University, Al-Hassa 31982, Saudi Arabia
[4]Physics Department, Faculty of Science, Ain Shams University, Cairo, Egypt
[5]Physics and Astronomy Department, College of Science, King Saud University, P.O. Box 2455, Riyadh 11451, Saudi Arabia.
* youssifm@yahoo.com

Abstract: Photoacoustic and AC impedance measurements of *ZnO* varistors with *ZnO* nanoparticles addition (≤ 150 nm) are performed by using gas-microphone detection method and precision impedance analyzer, respectively. It is found that the energy gap E_g is slightly decreased from 3.07 eV, for pure sample, to 2.96 eV with increasing *ZnO* nanoparticles additions up to 50%, followed by an increase of E_g up to 3.07 eV with further increase of *ZnO* nanoparticles up to 100%. However, these samples have different shapes of spectrum depending on *ZnO* nanoparticles addition, such as one semicircle, two semicircle, one arc as one quarter of a circle and two arcs. We have found that the conductivity of grains is nearly about 10^3 times more than the conductivity of the grain boundaries. The conduction in the grains and grain boundaries occurs in the same process for the additions with 5%, 10%, 50%, and could not be separated by the impedance spectroscopy. Although the dielectric constant is not systematic with *ZnO* nanoparticles addition, it is generally improved by the additions. Our results are discussed in terms of the nano size of the grains which are localized at the grain boundaries of *ZnO*.
[A. Sedky M. I. Youssif and T. A. El-Brolossy. **Photoacoustic and Ac Impedance Measurements for ZnO Varistors with ZnO Nanoparticles Addition.** *Nat Sci* 2016;14(2):66-73]. ISSN 1545-0740 (print); ISSN 2375-7167 (online). http://www.sciencepub.net/nature. 9. doi:10.7537/marsnsj14021609.

Keywords: Nanoparticles; *ZnO* nanoparticles addition; Photoacoustic; Dielectric Constant; Ac-Impedance

1. Introduction

Zinc oxide *(ZnO),* a wide band-gap semiconductor with large exciton binding energy (about 60 mV) is one of the most promising semiconductor materials for its applications in various areas such as optoelectronics [1], spintronics [2], piezoelectric transducers [3], ultraviolet optoelectronics [4]. It is commonly accepted that Polycrystalline *ZnO* ceramic with additives exhibits nonlinear current-voltage (I-V) characteristics due to the electrostatic potential barriers formed at grain boundaries [5-9]. The existence of the nonlinearity region is the most significant property of the varistors as a result of its conducting phase in this region. Although lot of works have been done in the I-V studies of *ZnO* varistors, a few investigations have been carried out on the optical absorption measurements because of difficulty of conventional transmitting methods [10]. It is necessary to get information about optical absorption of *ZnO* varistors for more investigations on their electronic states, and also band gap determination. However, three different values (3.1, 3.2 and 3.3 eV) have been reported for the optical band gap of *ZnO* single crystals at room temperature as well as free exciton energy of (40-60 mV) [11, 12].

Photoacoustic technique (PA) is a photo-thermal detection method that has proved to be a powerful tool for investigating the optical and thermal properties of materials by measuring the non-radiative de-excitation processes that follow optical absorption [13-16]. One of the significant advantages of the PA technique is that it is a non-contact and non-destructive method, and requires no particular sample treatment. Moreover, PA spectra are rather insensitive to light scattering effects in powder samples. PA technique provides the easy and reliable method for optical absorption spectra of opaque samples. In this work, we have used PA technique to study the optical absorption and measure energy band gap (E_g) of *ZnO* ceramics.

It is well known that electron traps, localized at the grain boundaries of *ZnO* ceramics, are adsorbed oxygen and capture the electrons coming from the donor states [17]. As a result of these traps, the Schottky barrier capacitance becomes dependent on the signal frequency of measurements. This is due to the finite time constants associated with the charging and discharging of the deep trap states in the depletion layer [18]. One way of studying the exchange phenomena is by following the harmonic response under low ac voltages [19]. When a time dependent voltage (≈ 300 mV) is applied across a ceramic sample, a sinusoidal current will flow with the same

angular frequency [20]. Ac impedance spectroscopy is a powerful technique for the characterization of grain boundaries in ceramic materials. It has the great advantage over the dc techniques of being able to separate the electric response in different regions of *ZnO* ceramics, provided their electrical responses within the range of the instrumentation and the time constants [21]. This response in the linear region is entirely characterized by the complex impedance Z as a function of the frequency (ω). The real and imaginary parts of Z (Z' and Z'') with respect to the applied voltages can be determined in the frequency range up to GHz. The frequency of the capacitance response can be obtained from the dielectric constant of *ZnO* varistors versus frequency. Furthermore, the resistance of both grains and grain boundaries can be determined from Z'' versus Z' plot.

In the last few years, progress has been achieved in synthesis, structural characterization and physical properties of nanostructures. These nanomaterials, due to their peculiar characteristics and size effects often show novel physical properties compared to the bulk samples. Today, nanoparticles of metal oxides have been the focuses of a number of research efforts due to the unusual properties that are expected upon entering this size regime [22]. Recently, structural, I-V characteristics and temperature dependent conductivity of *ZnO* samples with various nanoparticles addition are investigated [23]. In the present work, photoacoustic and AC impedance analyzer measurements are performed in order to investigate the optical absorption and measure energy band gap (E_g) of *ZnO* ceramics with various *ZnO* nanoparticles addition (5%, 10%, 30%, 50%, 75%, and 100%).

2. Experimental details

ZnO ceramic samples with various *ZnO* nanoparticles addition (5%, 10%, 30%, 50%, 75%, and 100%) are synthesized by using conventional solid-state reaction method [23]. Briefly, powders of *ZnO* and *ZnO* nanoparticle size (≤ 150 nm) of 99.99% purity (Sigma-Aldrich product) are thoroughly mixed in required proportions and calcined at 900 ^{0}C in air for a period of 12 hours. The resulting powders are ground and pressed into pellets of 1 cm diameter and 0.3 cm thick. These pellets are sintered at temperatures of 1000^{o}C for 10 h in air, and then quenched in air down to room temperature. The bulk density of the samples is measured in terms of their weight and volume. The phase purity and surface morphology of all samples are examined by using X-ray powder diffraction (XRD) at room temperature in the angle range 2θ = 10– 70° with the characteristic Cu K_α radiation and graphite monochromator. PA measurements are carried out by gas-microphone detection method. A monochromatic light beam from Xenon arc lamp through a monochromator is modulated with a mechanical chopper and focused on the surface of a sample placed inside a sealed PA cell. The light absorbed by the sample is converted into heat by non-radiative relaxation process and results in pressure fluctuations in the air inside the cell which can be detected by the microphone enclosed in the PA cell. The PA signal from the microphone is measured by a lock-in amplifier (SR 830). High-quality carbon black has been used for signal normalization. Finally, the ac impedance at room temperature is measured by using precision impedance analyzer model 4295A (40–110 MHz). The modulus of complex impedance Z and phase angle as a function of frequency (ω) are well recorded. From the impedance spectra, values of the real Z' and the imaginary Z'' parts of the complex impedance could be obtained.

3. Results and Discussion

3.1 Optical band gap

X-ray powder diffraction (XRD) pattern for *ZnO* samples with different *ZnO* nanoparticles content (5%, 10%, 30%, 50%, 75%, and 100%) is shown in Figure 1. It is clear that the crystal structure of all samples is hexagonal wurtzite structure, and no additional lines could be formed with *ZnO* nanoparticles addition up to 100%. The well known peaks of *ZnO* such as (100), (002), (111), (102), (110), (103), (200) and (112) are formed. *ZnO* behaves as n-type semiconductor, as its conduction band arises from the 4s orbital of *Zn* is wide enough to favors the effective charge transfer. Electrons are excited from its valence state, due to the absorption of light of this process, generates the electron-hole pairs which starts the conduction mechanism. Above the band gap energy limit, the photon energy signal is due to non-radiative process and that of below it is due to the Urbach Tail [24]. The dependence of the optical absorption coefficient, β, of a material on the incident photon energy, $h\nu$, has been formulated by Tauc's relation [25] as:

$$\beta h\nu = C\,(h\nu - E_g)^m \qquad (1)$$

The parameter C is a constant related to the electronic transition probability and m is the power which characterizes the type of transition process, m = *1/2* and *3/2* for direct allowed and forbidden transitions, respectively; and m = *2* and 3 for indirect allowed and forbidden transitions, respectively. The best fit for our data is found to be with the value of m = *1/2*, indicating that the dominant transition is direct allowed transition. Therefore, for band-gap energy E_g determination, we have assumed that the fundamental absorption edge of *ZnO* is due to the direct allowed transition. Accordingly, by using equation (1), β varies with the excitation light energy $h\nu$, and is given near the band gap by the following expression [26]:

$(\beta h\nu)^2 = C\,(h\nu - E_g)$ (2)

Here E_g is the direct allowed energy gap. The PA phonon signal intensity ρ is directly proportional to β and hence $(\rho h\nu)^2$ is related to $h\nu$ linearly. Figure 2, illustrates the spectral distribution of phonon signal intensity $(\rho h\nu)^2$ as a function of the incident photon energy, $h\nu$. The value of E_g is obtained by extrapolating the linear fitted regions to $(\rho h\nu)^2 = 0$. The behavior of the optical band gap E_g of *ZnO* ceramic samples with various *ZnO* nanoparticles addition (5%, 10%, 30%, 50%, 75%, and 100%) is shown in Figure 3. By observing this figure, it is obvious that the energy gap E_g is slightly decreased from 3.07 eV, for pure sample, to 2.96 eV with increasing *ZnO* nanoparticles additions up to 50%, followed by an increase of E_g up to 3.07 eV with further increase of *ZnO* nanoparticles up to 100%. These values are in consistent with the reported data elsewhere [10-12, 27, 28]. Moreover, this behavior is typically similar to the behavior of the activation energy against doping content in the region close to room temperature (300-420 K). Furthermore, the value of E_g for pure *ZnO* micro sample is the same as of *ZnO* nanoscale (E_g = 3.07 eV for both samples). These results are in good agreement with the behavior of the activation energy versus nanoparticles content discussed in earlier work [23]. However, the optical results are considering main evidence supporting the electrical measurements. Based on these results, the value of E_g is around 3.0 eV for all samples, which indicates that the probability of *ZnO* nanoscale substitution into the grain boundaries is very low at the considered sintering temperature. In fact, there are a variety of some other intergrain conduction paths that operate in parallel [5, 10], such as through the bulk intergranular material or through the grain boundary region are sensitive to the presence of *ZnO* nanoparticles. These paths could be providing small potential barriers to give linear I-V behavior for the present varistors, in agreement with the earlier I-V characteristics investigation [23], where we have got linear behavior for all the nanoparticle samples.

3.2 Ac Impedance Measurements

The representation of the complex impedance $Z(\omega)$ is given by:

$Z(\omega) = Z'(\omega) - j\,Z''(\omega)$ (3)

where $Z'(\omega)$ and $Z''(\omega)$ are the real and the imaginary parts of the ac complex impedance, respectively. However, by using Debye model, the impedance spectrum is in semicircle centered on the real axis and the relaxation time τ_o is unique. This model is expressed by [29, 30]:

$$Z(\omega) = Z^*_\infty + \frac{Z^*_{0\infty}}{1 + j\omega\tau_0} \quad (4)$$

Where $Z^*_{0\infty}$ is the impedance at infinite frequency, $Z^*_{0\infty} = Z^*_0 - Z^*_\infty$, $Z^*_0 = Z^*_0(\omega)$, $as\ \omega \to 0$, where $\omega = 2\pi f$, and τ_o can be calculated from $\omega\tau_o = 1$ at the summit of the semicircle [31].

In case of Cole-Cole model, the impedance representation is given by a circular arc centered below the real axis $Z^*(\omega)$, and the relaxation time constant is dispersed. Thus, there is a depression angle θ between the real axis and the straight line defined by the origin of axis and the center of the circle containing the arc. This model is expressed by the following empirical relation [29-31]:

$$Z(\omega) = Z^*_\infty + \frac{Z^*_{0\infty}}{1 + (j\omega\tau_p)^{1-\gamma}} \quad (5)$$

Where $\gamma = (2\theta/\pi)$ and $(1 > \gamma > 0)$, which can be determined experimentally, and τ_p is the most probable relaxation time which can be calculated from $\omega\tau_p = 1$ at the summit of the arc [32]. However, it has been found that the impedance spectra of pure nanophase *ZnO* (without sintering) exhibited two arcs. The first arc at a low frequency is interpreted due to the grain boundary effect while the second arc at a high frequency region is attributed to the grain's effects [33-36]. The impedance spectra for sintered and doped *ZnO* ceramics have been studied and only a single arc is observed in all spectra [37, 38]. In literature, some researchers [34] though the single arc spectrum means that the conduction processes through the grain and grain boundary had identical time constants, $\tau = (1/\omega) = RC$, which indicates that the conduction in the grain and grain boundary occurs in the same process and could not be separated by the impedance spectroscopy [39]. On the other hand, other researcher groups [37] think that the single arc is due to the contribution from resistive grain boundary and conducting grain cores. Furthermore, it has been observed from complex impedance measurements that *Mn* ($Mn \geq 0.30$) induces a grain boundary semicircle in the impedance spectra of *ZnO* [40, 41]. However, the impedance spectra of pure and *0.10 mole % Mn* are devoid from any grain boundary semicircle. This fact suggests that excess *Mn* probably exists in the grain boundary region, either as a very thin second phase or as an amorphous film, which could benefit the grain boundary transport for grain growth. The measurements of the Ac impedance have been made on nanocrystalline *ZnO* ceramics at frequencies ranging from 10 Hz to 1.2 MHz at room temperature [42]. Only one arc for resistive grain boundary is recorded while the other arc for the grain interior is so small to be imperceptible. Figure 4 shows the real part of the ac impedance versus imaginary part at different frequencies. It is clear that these samples have

different shapes of spectrum depending on *ZnO* nanoparticles additions, such as one semicircle, two semicircle, one arc as one quarter of a circle and two arcs. From these curves, the average grain and grain boundary conductivities are calculated and summarized in Table 1. As evidenced in Table 1, the conductivity of grains is about 10^3 times more than the conductivity of the grain boundaries. The conduction mechanisms in the grain and grain boundary occurs in the same process for 5%, 10% and 50% samples, and could not be separated by the impedance spectroscopy in agreement with the reported data [39]. Moreover, the conductivity of *ZnO* samples with nanoparticles addition is higher than that of pure *ZnO* sample. The dielectric constant as a function of frequency *(ln f)* for pure and with *ZnO* nanoparticles addition samples is represented in Figure 5. Although the dielectric constant values are not systematic with the *ZnO* concentration, it is generally improved by the nanoparticles addition, in good agreement with the results of conductivity for these samples, Table 1. Based on these results, we can gather conclude that the probability of *ZnO* nanoscale substitution into the grain boundaries is very high at the considered sintering temperature. The nanosize grains are able to localize at the grain boundaries, and helps for producing some other sensitive intergrain conduction paths. These conduction paths can operate in parallel [12, 43] through the grain boundary region and completely deformed the potential barriers of *ZnO* varistors. These results are in good agreement with I-V characteristics, where we have got linear behavior for all *ZnO* nanoparticle samples.

Table 1: Optical band gap versus *ZnO* nano content for *ZnO* samples

ZnO nanoparticles addition	E_g (eV)	Average cond. $(ohm.cm)^{-1}$	Grain cond. $(ohm.cm)^{-1}$	Grain boundary cond. $(ohm.cm)^{-1}$
0.0%	3.07	$2.54x10^{-7}$	----------	--------
5%	3.05	$58x10^{-7}$	$10x10^{-3}$	$34x10^{-6}$
10%	3.01	$31x10^{-7}$	$6.25x10^{-3}$	$1.74x10^{-6}$
30%	2.98	$27x10^{-7}$	$9.09x10^{-3}$	$1.67x10^{-6}$
50%	2.96	$12x10^{-7}$	--------	---------
75%	2.97	$169x10^{-7}$	$4x10^{-3}$	$94.3x10^{-6}$
100%	3.07	$49x10^{-7}$	$11.77x10^{-3}$	$3.17x10^{-6}$

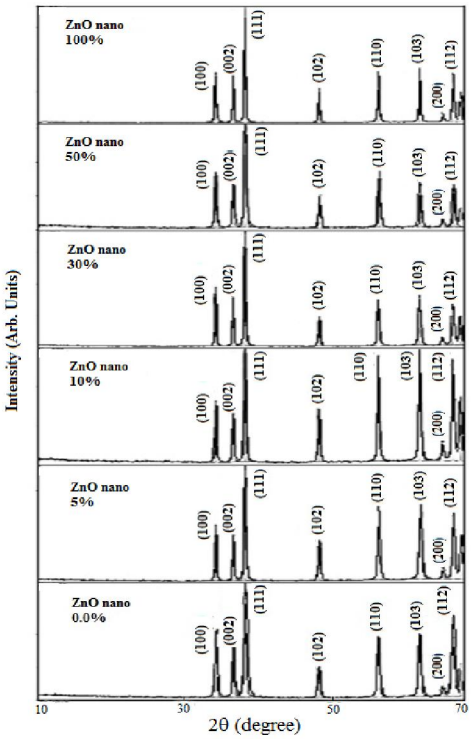

Figure 1: XRD pattern for ZnO samples with different ZnO nanoparticles content

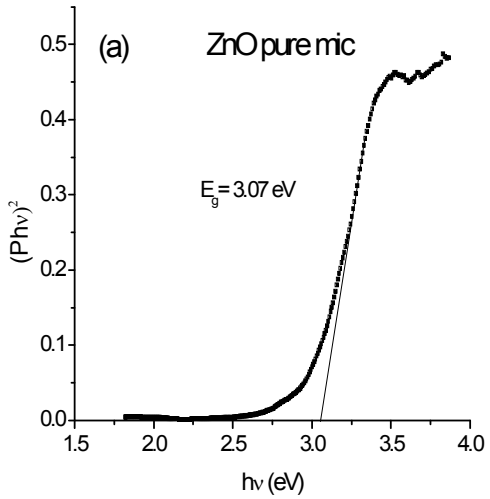

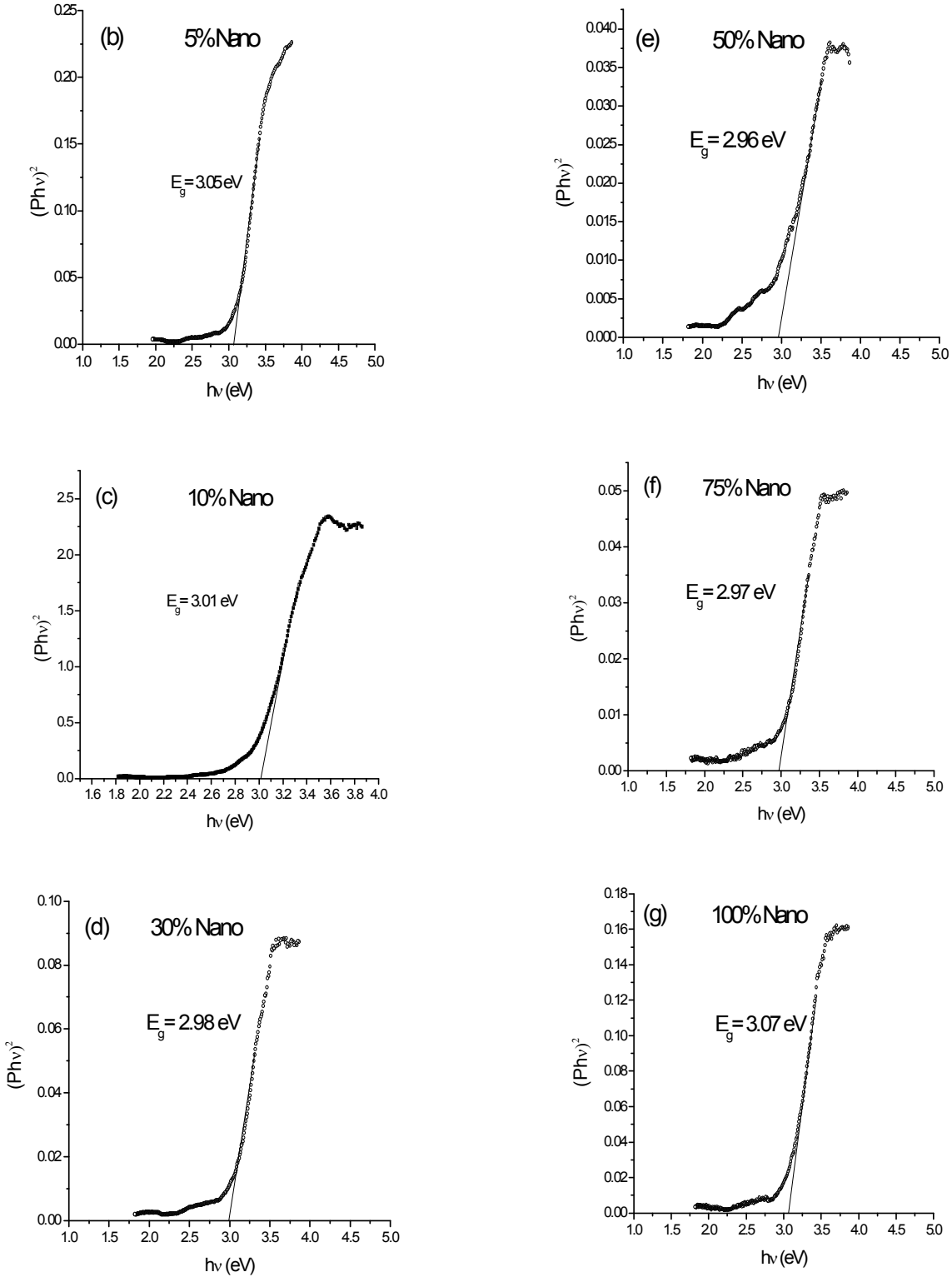

Figure 2: Optical intensity $(\rho hv)^2$ versus photon energy (hv) for *ZnO* samples with different *ZnO* nanoparticles content

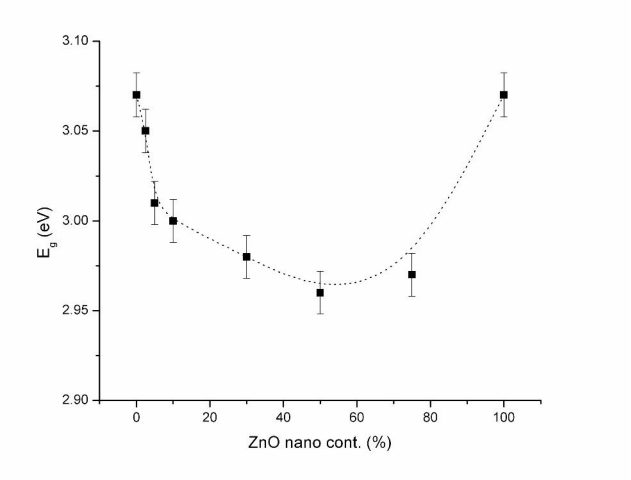

Figure 3: Optical band gap versus *ZnO* nano contents for *ZnO* samples

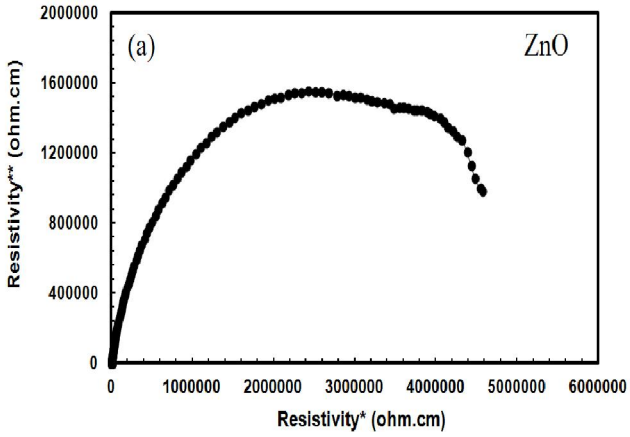

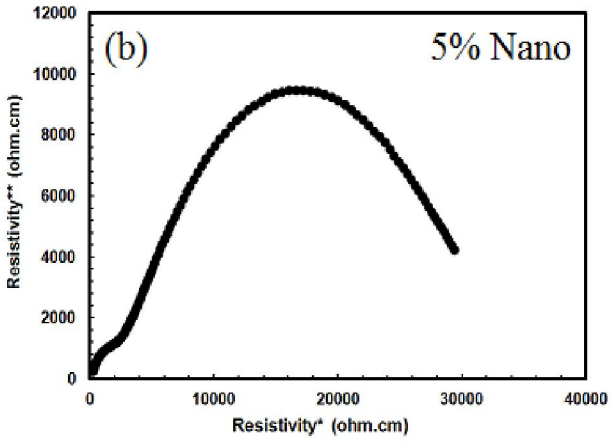

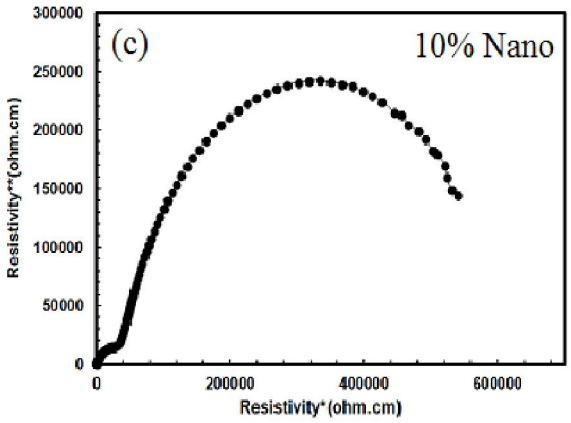

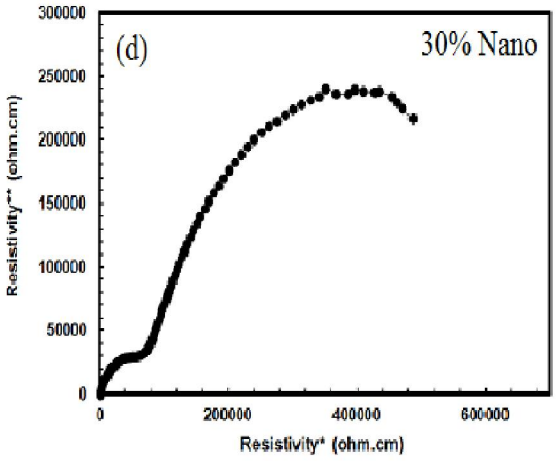

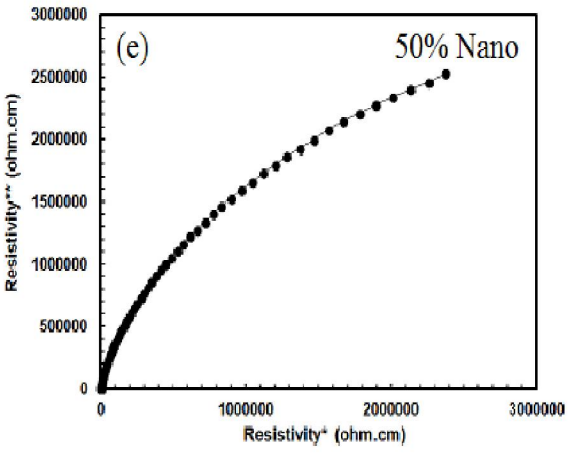

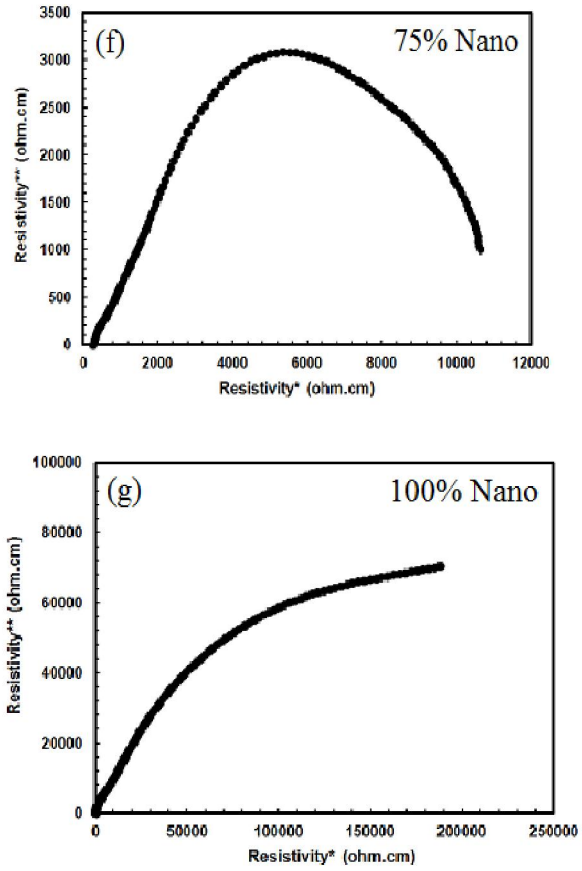

Figure 4: Cole- Cole measurements for *ZnO* samples with different *ZnO* nanoparticles content.

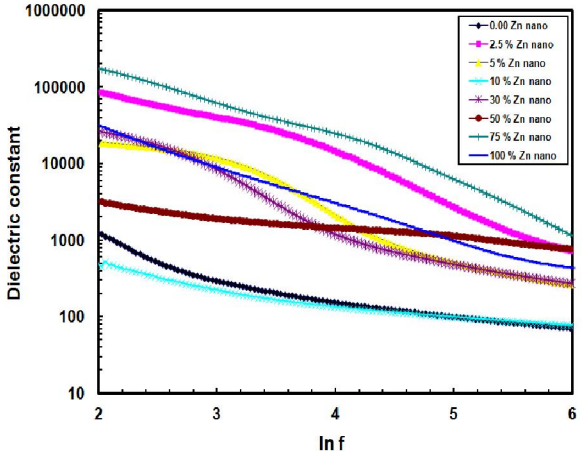

Figure 5: Dielectric constant versus *lnf* for *ZnO* samples with different *ZnO* nanoparticles content.

4. Conclusion

Photoacoustic and AC impedance measurements of *ZnO* varistors with *ZnO* nanoparticles addition (≤ 150 nm) are performed by using gas-microphone detection method and precision impedance analyzer, respectively. For band-gap energy E_g determination, it is found that the fundamental absorption edge of *ZnO* is due to direct allowed transition. Values of the energy gap E_g have been found to strongly depend on *ZnO* nanoparticle's content. Moreover, Cole- Cole measurements have different shapes of spectrum depending on *ZnO* nanoparticles additions. Ac impedance shows only one arc for resistive grain boundary while the other arc for the grain interior is so small to be imperceptible. Based on the fact that the values of E_g is around 3.0 eV for all samples, make us to believe that the probability of *ZnO* nanoscale substitution into the grain boundaries is very low and there are a variety of some other intergrain conduction paths could provide small potential barriers to give the linear I-V behavior for the present varistors. We have found that the conductivity of grains are nearly about 10^3 times more than the conductivity of the grain boundaries as well as the conduction in the grains and grain boundaries occurs in the same process for the addition with 5%, 10%, 50% and could not be separated by the impedance spectroscopy. As a general behavior, values of the dielectric constant are improved by *ZnO* nanoparticles addition in agreement with the results of the conductivity for these samples. These results are discussed in terms of the nano size of grains which are localized at the grain boundaries of *ZnO*.

References

1. Kong X. Y. and Z. L. Wang, Appl. Phys. Lett. 84, 6, pp. 975977 (2004).
2. Sharma P., A. K. Gupta, V. Rao, F. J. Owens, R. Sharma, R. Ahuja, J. M. Osorio, B. Johansson and G. A. Gehring, Nature Material 2, 10, pp. 673677 (2003).
3. Catti M., Y. Noel and R. Dovesi, J. Phys. Chem. Solids 64, 11, pp. 21832190 (2003).
4. Wang X., Y. Ding, C. J. Summers and Z. L. Wang, Journal of Physical Chemistry: B 108, pp. 87738777 (2004).
5. Matsouka M., Jpn. J. Appl. Phys. 10, 6, 736 (1971).
6. Mukae K., K. Tsuda and I. Nagasawa, Jpn. J. Appl. Phys. 16, 8, 1361 (1977).
7. Pike G. E. and C. H. Seager, J. Appl. Phys. 50, 5, 3414 (1979).
8. Fumiyasu Obe, Yukio Sato, Takahisa Yamamoto, Yuichi Ikuhara and Taketo Sakuma, J. Am. Ceram. Soc. 86, 9, 1 (2003).
9. Zhen Zhou, K. Kato, T. Komaki, M. Yoshino, H. Yukawa, M. Morinaga and K. Morita, J. Eur. Ceram. Soc. 24, 139 (2004).
10. Azmi B. Z., Zahid Rizwan, M. Hashim, A. H. Shaari, W. M. M. Yunus and E. Saion, Am. J. Appl. Sci. (Special Issue) 22 (2005).

11. Srikant V. and D. R. Clarke, J. Appl. Phys. 83, 10, 5447 (1998).
12. Azmi B. Z., Zahid Rizwan, M. Hashim, A. H. Shaari, W. M. M. Yunus and E. Saion, Am. J. Appl. Sci. (Special Issue), 22 (2005).
13. Shen Q., T. Toyoda, Jpn. J. Appl. Phys. 39, 511 (2000).
14. Shen Q., T. Toyoda, Jpn. J. Appl. Phys. 39, 3146 (2000).
15. Abdalla S., K. Easawi, T. A. El-Brolossy, G. M. Yossef, S. Negm and H. Talaat, Rev. Sci. Instrum., 74 (1), 848 (2003).
16. El-Brolossy T. A., S. Abdalla, O. E. Hassanein, S. Negm and H. Talaat, J. Phys. IV France, 125, 685 (2005).
17. Sleston L. C., M. E. Potter and A. M. Alim, J. Am. Ceram. Soc. 71, 909 (1987).
18. Eizinger, Surf. Sci. 1, 329 (1978).
19. ezhilvalavan and T. R. N. Kutty, Appl. Phys. Lett. 69, 23, 3540 (1996).
20. Agnes Smith, Jean Francois baumard and Pierre Abelard, J. Appl. Phys. 65, 2, 5119 (1989).
21. M. Andres Verges and A. R. West, J. Electroceramics 1:2, 125 (1997).
22. M. L. Dinesha, H. S. Jayanna, S. Ashoka and G. T. Chandrappa, J. Alloys Comp. 485, 538 (2009).
23. A. Sedky and Abdullah Aljaafari, the XXXI International Conference on MaterialsScience and Applications, Hurghada, Egypt, January (2015).
24. Kimura, Y. Ohbuchi, T. Kawahara, Y. Okamoto and J. Morimoto, Jpn. J. Appl. Phys. 40, 3614 (2001).
25. J. Tauc "Amorphous and liquid semiconductors" plenum press, London, 1974.
26. T. Toyoda, H. Nakanishi, S. Endo and T. Irie, J. Phys. D: Appl. Phys. 18, 747 (1985).
27. G. D. Mahan, L. M. Levinson, H. R. Philipp, J. Appl. Phys. 50, 2799 (1979).
28. L. K. J. Vanadamme and J. C. Brugman, J. Appl. Phys. 51, 4240 (1980).
29. K. H. Cole and R. H. Cole, J. Chem. Phys. 9,341 (1941).
30. K. Al Abdullah, A. Bui and A. Loubiere, J. Appl. Phys. 69, 7, 4046 (1991).
31. R. Bartnikas and R. M. Eichhorn, eds. Engineering Dielectrics (ASTM), Philadelphia IIA, 69 (1983).
32. Y. Duit, J. Appl. Phys. 14, 939 (1979).
33. J. Jose and Abdul Khadar, Mater. Sci. Eng. A (304-306), 810 (2001).
34. J. Jose and Abdul Khadar, Nanostruct. Mater. 11, 8, 1091 (1999).
35. J. Jose and Abdul Khadar, Acta Mater. 49, 729 (2001).
36. W. C. Nan, A. Tschope, S. Holten, H. Kliem and R. Birringer, J. Appl. Phys. 85, 11, 7735 (1999).
37. Z. Brankoviz, G. Brankoviz, D. Poleti and A. J. Varela, Ceram. Int. 27, 1, 115 (2001).
38. Glot, E. Bartolomeo and E. Traversa, Eur. Ceram. Soc. 19, 715 (1999).
39. Zhen Zhou, K. Kato, T. Komaki, M. Yoshino, H. Yukawa, M. Morinaga and K. Morita, J. Eur. Ceram. Soc. 24, 139 (2004).
40. J. Han, P. Q. Mantas and A. M. R. Senos, J. Eur. Ceram. Soc. 20, 2753 (2000).
41. J. Han, A. M. R. Senos and P. Q. Mantas, Mater. Chem. Phys. 75,117 (2002).
42. Lian Gao, Qiang Li and Weiling Luan, J. Am. Ceram. Soc. 85, 4, 1016 (2002).
43. L. M. Levinson and H. R. Phillip, Am. Cream. Soc. Bull. 65 (4), 639 (1986).

2/2/2016